RSC Advances

ROYAL SOCIETY OF CHEMISTRY

www.rsc.org/advances

Heterogeneous phase formation in diluted magnetic semiconducting $Zn_{1-x-y}Co_xAl_yO$ (CAZO) nanoparticles

R. Siddheswaran[a*], R. Medlín[a], P. Bělský[a], V. Vavruňková[a], J. Očenášek[a], Bohumil David[b], and P. Šutta[a]

[a]New Technologies Research Centre, University of West Bohemia in Pilsen, Plzeň-30614, Czech Republic.
[b]CEITEC IPM, Institute of Physics of Materials, ASCR, v.v.i., Žižkova 22, CZ-61662 Brno, Czech Republic.
E-mail: ***rsiddhes@yahoo.com, rajendra@ntc.zcu.cz***

Image for graphical abstract:

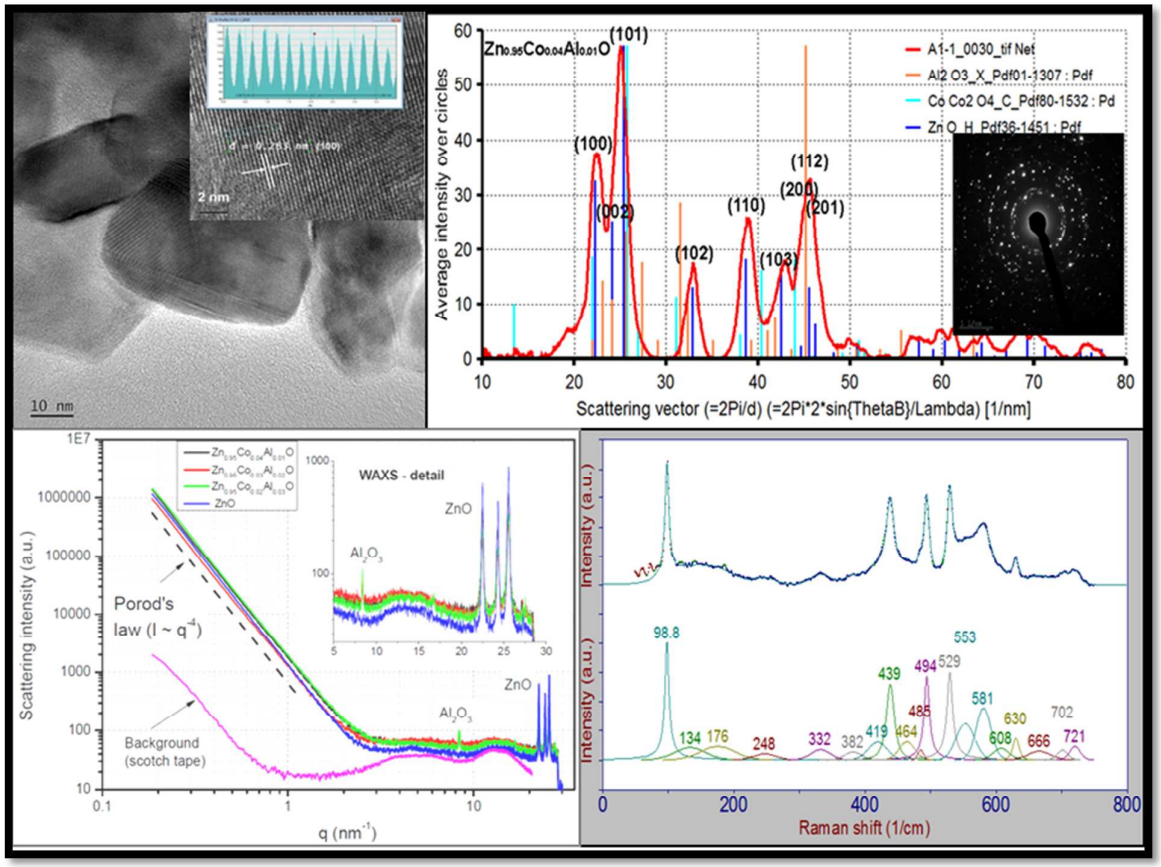

RSC Advances

RSCPublishing

ARTICLE

Heterogeneous phase formation in diluted magnetic semiconducting $Zn_{1-x-y}Co_xAl_yO$ (CAZO) nanoparticles

Cite this: DOI: 10.1039/x0xx00000x

R. Siddheswaran[a*], R. Medlín[a], P. Bělský[a], V. Vavruňková[a], J. Očenášek[a], Bohumil David[b], and P. Šutta[a]

Received 00th xxxxx 2014,
Accepted 00th xxxxx 2014

DOI: 10.1039/x0xx00000x

www.rsc.org/

This article reports a systematic investigation of the synthesis and structural characterization of a composite CAZO [($Zn_{1-x-y}Co_xAl_yO$; x=0.04, 0.03, 0.02; y=0.01, 0.02, 0.03)] nanoparticles from combustion. The crystalline phase, morphology, size, and structure were characterized using X-ray diffraction (XRD), small and wide angle X-ray scattering (SAXS/WAXS), scanning electron microscopy (SEM) and high resolution transmission electron microscopy (HR-TEM). The XRD and SAXS/WAXS analyses confirm the formation of Co and Al co-doped ZnO hexagonal wurtzite structure with additional metal oxides phase. The particle size and micro-strain were calculated by means of an integral breadth of X-ray diffraction lines. The selected area electron diffraction (SAED) patterns from TEM were correlated with the XRD patterns. The energy dispersive X-ray spectra (EDX) from SEM/TEM were recorded in order to analyze the composition of elements in the composite. The vibrational modes of the functional groups presented in the materials were assigned from FTIR and Raman spectra. The magnetic hysteresis measurement confirmed the room temperature ferromagnetism.

1. INTRODUCTION

Zinc oxide is a significant II–IV n-type semiconductor with wide electronic band-gap (Eg=3.37 eV) and large free exciton binding energy (60 meV). Hence, it has been considered as a good candidate for various applications, for example, gas sensors, photo-catalysts, ceramics, microwave absorbers, varistors, piezoelectric transducers, short wavelength optical devices, solar cell windows, optical wave guides and spintronic devices.[1–9] One of the recent studies of room temperature ferromagnetism in diluted magnetic semiconductors has stimulated a great research interest for its potential applications in spintronics and optoelectronics.[10] ZnO nanostructures provide several opportunities for researchers to explore the unique properties and applications. For semiconductors, doping and incorporation of metal elements is a powerful tool to tailor the electrical and optical properties for the construction of many optoelectronic devices. More interestingly, in previous theoretical studies and experimental results have showed that ZnO doped with appropriate transition metals were considered as diluted magnetic semiconductors[11–15] which attracted a lot of interest due to their ferromagnetism at room temperature. Thus, zinc oxides of different morphologies with different dopant combinations are significant and their applications are growing up. It is well known that ZnO materials are widely used in various fields of science and technology using different preparation methods.[16–23] Among the methods, combustion synthesis has many potential advantages such as low processing cost, energy efficiency, relative simplicity, high production rate, etc.[21, 24, 25] In our previous study,[14] a combustion synthesis process was developed for the synthesis of $Zn_{1-x-y}Co_xAl_yO$ (CAZO) nanoparticles, where only the single phase formation was detected based on fast-scan XRD. Within present paper, we report in-depth analyses of the crystalline phase formation by slow-scan XRD, SAXS/WAXS and SAED profile fitting. Also, the surface morphology, particle size distribution, elemental analyses and spectroscopic studies were carried out.

2. MATERIALS AND METHODS

Preparation of [($Zn_{1-x-y}Co_xAl_yO$; x=0.04, 0.03, 0.02; y=0.01, 0.02, 0.03)]: Initially, the CAZO nanoparticles were synthesized by citrate nitrate auto-combustion (CNA) method using zinc nitrate [$Zn(NO_3)_2$ $6H_2O$], cobalt nitrate [$Co(NO_3)_2$ $6H_2O$], and aluminium

nitrate [$Al(NO_3)_3\ 9H_2O$] as precursors, and citric acid [$C_6H_8O_7$] as a fuel. The stoichiometric proportions of precursor metal nitrates were dissolved in de-ionized water. The amount of organic fuel (citric acid) was calculated from the basic principle of propellant chemistry[26] to be added with the nitrates solution. The mixed solution was stirred well for 2 hours at 60 ºC to achieve homogeneity, afterwards transferred to platinum crucible and kept in a closed furnace maintaining a constant temperature of 500 ºC. The combustion reaction was completed in a time span of 10 minutes and porous solid foam of nanopowders was obtained. The assumed reaction held during the combustion process can be written as:

$$(1-x-y)[Zn(NO_3)_2\ 6H_2O] + x[Co(NO_3)_2\ 6H_2O] + y[Al(NO_3)_3\ 9H_2O] + (0.5583)_{x=0.04,y=0.01},(0.5611)_{x=0.03,y=0.02},(0.5639)_{x=0.02,y=0.03}[C_6H_8O_7] \xrightarrow{-\Delta} [Zn_{1-x-y}Co_xAl_yO + (N_2+CO_2+H_2O)\uparrow] \rightarrow \text{equ. (1)}$$

the equation (1), the reactant mixture was set at the condition that the value of oxygen balance is equal to zero. That is, the oxidizer (the NO_3 from the metals nitrate) completely and equivalently reacts with the fuels (i.e., Zn, Co and Al with citric acid) without requiring oxygen from any external source.[27] The combusted foams were crushed to obtain the nanopowder and then calcined at 600 ºC for 2 hours to obtain a fully crystalline powder.

Characterization: The X-ray diffraction experiments were carried out using an automatic powder X-ray diffractometer X'Pert Pro (PANalytical) equipped with an ultra-fast linear semiconductor detector PIXcel. Copper K_α radiation ($\lambda = 0.154$ nm) was used as an X-rays source. The ceramic alumina from NIST (National Institute of Standards and Technology) was used as an instrumental standard.

The structure of the powder samples was investigated by small and wide angle X-ray scattering (SAXS/WAXS) using the SAXSess mc^2 instrument (Anton Paar). The device uses a GeniX Microfocus X-ray point source with a Cu anode (50 kV and 1 mA), single-bounce focusing X-ray optics and an advanced collimation block. The experiments were performed in the standard transmission setup (perpendicular incidence) and imaging plates were used as detector. The scattering vector range used for the experimental setup was 0.18−28 nm^{-1}, i.e., it covered both the SAXS and WAXS range simultaneously. The scattering vector q is defined as $q = (4\pi/\lambda)\sin(2\theta/2)$, where λ is the X-ray wavelength and 2θ is the scattering angle (with respect to the incident beam). The sample exposition time was 10 min. The powders were first glued in between two pieces of scotch tape which then was fixed in the sample holder. The spectrum of the scotch tape was measured as background. The 1D radial intensity profiles were created from the measured 2D scattering images using the SAXS-quant software (Anton Paar). Due to the form of the samples (undefined thickness of the powder samples), it was not possible to calibrate the scattering intensities on the absolute scale and hence the data are presented in arbitrary intensity units (a.u.).

The morphological features of the CAZO were observed by a scanning electron microscope (FEI Quanta 200 equipped with EDX from EDAX) and the microstructures were recorded in detail using a high resolution transmission electron microscope (JEM-2200FS equipped with EDX X-Max from Oxford instruments). The Fourier transform infrared (FTIR) absorption spectra were recorded using Nicolet-380 FTIR spectrometer (Thermo Scientific) in the frequency range of 650–4000 cm^{-1} using ATR (Attenuated total reflection). Micro Raman spectroscopic analyses were performed using the DXR Raman spectrometer (Thermo Scientific) with wavelength of the incident beam 532 nm of Nd:YVO_4 DPSS laser source. The spectra were recorded for the wavenumber region 50–4000 cm^{-1}, but the CAZO absorbed and exhibited peaks only in the region 50–800 cm^{-1}. The ferromagnetic hysteresis of the CAZO nanopowders was measure using a physical properties measurement system (PPMS, Quantum Design) in VSM mode.

3. RESULTS AND DISCUSSION

Structural characterization by X-ray diffraction: The main structure parameters (crystallite size and micro-strains) of the CAZO powders were investigated by X-ray diffraction (XRD). Figure 1 shows the X-ray diffraction patterns of the CAZO synthesized with various Co and Al dopant levels. The diffraction peaks of (1 0 0), (0 0 2), (1 0 1), (1 0 2), (1 1 0), (1 0 3), (2 0 0), (1 1 2), (2 0 1) and (0 0 4) planes were observed for all samples. All the patterns fit well with the hexagonal wurtzite type structure corresponding to ZnO from the JCPDS card No: 00-036-1451. However, some additional phases corresponding to cobalt and aluminium species were detected. The X-ray diffraction pattern of $Zn_{0.95}Co_{0.02}Al_{0.03}O$ in comparison with different oxides of Zn, Al and Co is shown in Figure S1 of the supplementary information.

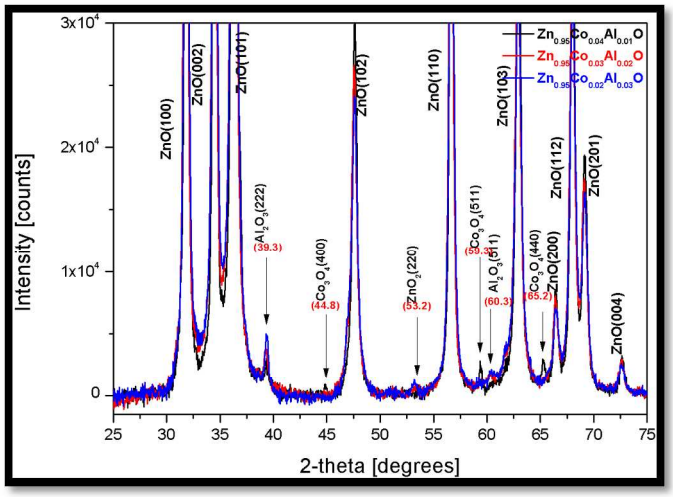

Figure 1. XRD pattern of the $Zn_{1-x-y}Co_xAl_yO$ (CAZO) nanocrystals.

According to JCPDS card No.00-01-1307, the weak diffraction peaks observed at angles 39.3º and 60.3º correspond to (222) and (511) planes of Al_2O_3, respectively. A relatively weaker diffraction peak observed at an angle 53.2º is indexed as (220) plane of ZnO_2 from the JCPDS card No.00-13-0311. Also, the weaker peaks

observed at angles 44.8º and 65.2º are indexed as (400) and (440) planes of Co_3O_4, respectively (JCPDS: 00-80-1532). But, these planes have comparatively negligible intensities rather ZnO planes. Shift in diffraction peaks and micro-strains were calculated with respect to the standard ZnO diffraction pattern. They are caused by interstitial or substitutional impurities (doping) of metal ions of Co and Al in the hosting sites. Since they exhibit majority of the peaks with higher intensities corresponding to ZnO planes, it is considered that the CAZO inherits the hexagonal wurtzite structure. Therefore, it is determined that the CAZO nanocrystals are formed as a composite of heterogeneous metal oxides.

Table 1. Size-Strain results of the CAZO powders.

Line (*h k l*)	$Zn_{0.95}Co_{0.04}Al_{0.01}O$		$Zn_{0.95}Co_{0.03}Al_{0.02}O$		$Zn_{0.95}Co_{0.02}Al_{0.03}O$	
	<*D*> [nm]	<ε> [-]	<*D*> [nm]	<ε> [-]	<*D*> [nm]	<ε> [-]
1 0 0	37	0.00251	35	0.00309	26	0.00290
0 0 2	30	0.00257	25	0.00330	18	0.00309
1 0 1	27	0.00223	23	0.00272	21	0.00313
1 0 2	19	0.00224	21	0.00303	19	0.00350
1 1 0	28	0.00140	30	0.00202	24	0.00202
1 0 3	18	0.00133	19	0.00226	21	0.00283
1 1 2	32	0.00179	24	0.00188	28	0.00249
2 0 1	24	0.00129	22	0.00170	25	0.00228
ϕ	~ 27	~1.9x10^{-3}	~25	~2.5x10^{-3}	~ 23	~2.8x10^{-3}

In powder X-ray diffraction, the position, height, integrated intensity and FWHM are the main four parameters that characterize the diffraction line profiles. The broadening of a diffraction line is a result of a real material structure, where the size of the crystallites and the micro-strains are the most important contributors to the broadening of the line. In this study we used a procedure utilizing an integral breadth of a diffraction line.[28,29] Equation (2) characterizes the integral breadth β that includes two parameters namely the intensity I_0 and the integral intensity.

$$\beta = \frac{1}{I_o}\int I(2\vartheta)\cdot \mathrm{d}(2\vartheta) \qquad \text{Equ. (2)}$$

There, $I_{\mathrm{int}} = \int I(2\vartheta)\cdot \mathrm{d}(2\vartheta)$ is the integral intensity (area below the line) and I_0 is the maximal intensity of the diffraction line $I(2\vartheta)$. In general, the instrumental resolution of the equipment has also to be taken into account in order to obtain a physical (depend only on the properties of the matter) component of the broadening of the diffraction line. Furthermore, the physical component of the integral breadth of the diffraction line is a convolution of Cauchy and Gaussian components and so it is necessary to perform de-convolution into a Cauchy β_C^f and a Gaussian β_G^f parts before the main real structural parameters are determined. The Cauchy and Gaussian parts of the integral breadth of the line correlate with the size of crystallites and micro-strains, respectively. The average crystallite size and micro-strains are determined using Equations (3) and (4), respectively.[29]

The average crystallite size <*D*> in the direction perpendicular to the diffracting lattice planes is

$$< D > = \frac{\lambda}{\beta_C^f \cos\vartheta}, \qquad \text{Equ. (3)}$$

where λ is the X-ray wavelength used and ϑ is the Bragg's angle.

The average micro-strain <ε> in the diffracting volume is defined as follows

$$< \varepsilon > = \frac{\beta_G^f}{4\mathrm{tg}\vartheta}. \qquad \text{Equ. (4)}$$

Evaluated crystallite size and micro-strains for the prominent diffraction planes are given in Table 1. It is observed that the particle size decreases with increase of aluminium content and the micro-strain increases with decrease of the particles size. This is due to smaller ionic radius of Al than Zn and Co.

Structural characterization by SAXS/WAXS analyses: The evolution of phase and size distribution of the CAZO particles can be extracted by fitting the SAXS/WAXS and the XRD patterns. Figure 2 shows the measured SAXS/WAXS profiles on a logarithmic scale. For all samples the intensity dependence in the SAXS range follows the Porod's law[30] very well (a power law with exponent equal to *–4: I ~ q*$^{-4}$) expressing a very good agreement with the theory for the high-q tail of scattering on particles with a sharp interface. (See the broken line at Figure 2 representing the Porod's law.) The average size of the particles was observed greater than 25 nm, which is determined based on the fitting of particle size distributions to the experimental data using *Irena* program.[31] It is a typical picture of small-angle scattering of a powder with no significant internal structure of the material at nanometer scale (from about 1 nm to 20 nm).

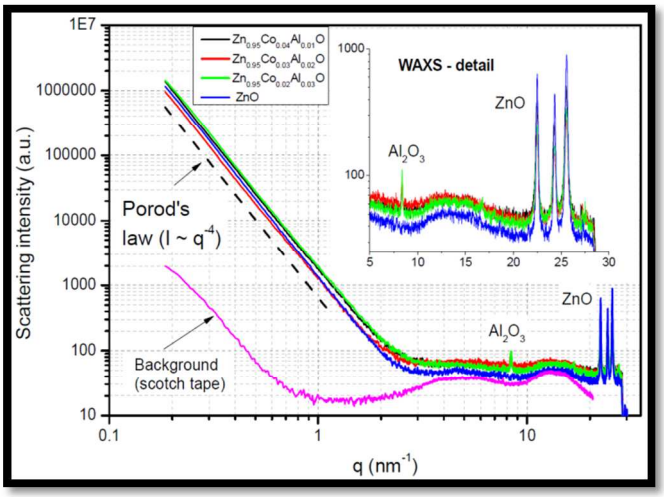

Figure 2. SAXS/WAXS pattern for the CAZO nanoparticles.

In the WAXS range, four diffraction peaks were observed. The three peaks at *q* values of 22.5, 24.3, and 25.5 nm^{-1} corresponding to 2θ angles of 32.0 (100), 34.7 (002), and 36.5º (101), respectively,

originated from the ZnO (JCPDS: 00-036-1451) and appeared for all samples (Figure 2). These peaks can also be seen in the graphs in Figure 1 from the XRD analysis. The peak at q = 8.37 nm^{-1} corresponding to 2 θ =11.8º (out of the range of the XRD analysis) indicates the (101) plane of the Al_2O_3 (JCPDS: 00-016-0394) and appeared for all the combinations of $Zn_{1-x-y}Co_xAl_yO$. The two small broad humps around 4.5 and 14 nm^{-1} were observed from the background (scotch tape), as can be seen by comparison with its spectrum. As explained in the experimental section, the scattering intensities are in arbitrary units and thus, a quantitative comparison of the phase composition of different samples cannot be compared directly. Nevertheless, quantitative analysis was done by means the XRD studies.

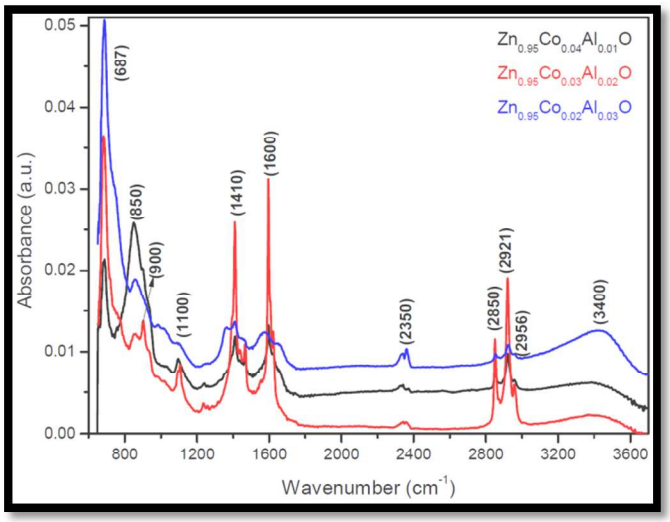

Figure 3. FTIR spectra of the CAZO at different Co and Al concentrations.

Fourier transform infrared spectroscopy (FTIR) analyses: The FTIR attenuated total reflectance (ATR) absorbance spectra of the CAZO samples are shown in Figure 3. The apprehended carbon and hydrogen during the combustion process and organic impurities (which might remain adsorbed on the surface of ZnO) due to sample processing are reasons to expect C–H and C–O modes in the FTIR spectrum of this material. The weak and broad asymmetrical absorption region at around 3400 cm^{-1} is likely due to the O–H vibrations from the physically absorbed moisture in ambient atmosphere. The C–H stretching modes of an aliphatic compound were observed between 2800 and 3000 cm^{-1}. The sharper absorption peaks at 2850 and 2921 cm^{-1} belong to symmetric and asymmetric vibrations of the methylene group. The small shoulder at 2956 cm^{-1} was assigned to methyl group. The weaker absorption peak observed at 2350 cm^{-1} is assigned to the CO_2 stretching vibration from ambient air. The absorption at ~1600 cm^{-1} was attributed to the carbonyl group (C=O, stretching vibration). A narrow strong peak at 1410 cm^{-1} belongs to plain bending mode of C–OH. Generally, similar C–H peaks have been observed in pure ZnO powders and single crystals.[32,33] In the spectral region with wavenumbers lower than 1100 cm^{-1} were assigned for the vibrations associated with Zn–O, Co–O and Al–O, but these band are also overlapping with other fingerprint absorptions of the molecules of multiple band structure in that region. The peak observed at 687 cm^{-1} was assigned to Al–O vibration modes in Zn–O. The peaks observed between 850 and 900 cm^{-1} are caused by Co–O in Zn–O vibrations.

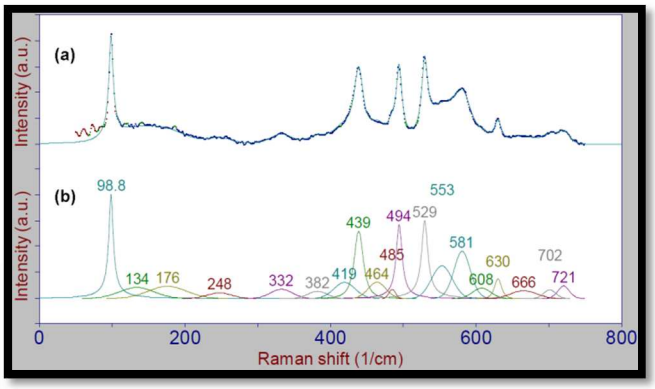

Figure 4. Raman spectrum of $Zn_{0.95}Co_{0.03}Al_{0.02}O$, a) experimental data and fitted spectrum, and b) decomposed fitted spectrum.

Raman spectral characteristics: The measured and fitted Raman spectra in Figure 4a), b) shows the decomposed spectrum after baseline correlation and decomposition by least-square fitting using Pearson´s VII area function for individual vibrational modes. ZnO wurtzite-type belongs to the space group C_{6V}^4. According to the group theory, it has eight sets of phonon vibration modes of $2E_2$, $2A_1$, $2E_1$ and $2B_1$.[34,35] Among them, the $2B_1$ modes are Raman inactive and infrared active (silent modes). The A_1 and E_1 polar modes are divided into transverse optical (TO) and longitudinal optical (LO) phonons (Raman and infrared active). Also, the two non-polar E_2 modes are Raman active. The Raman spectra of the CAZO with various doping concentration have similar vibrations as those shown in Figure S3.

The characteristic bands of the wurtzite ZnO peaks observed at 99 cm^{-1} and 439 cm^{-1} are assigned to E_2 (low) and E_2 (high) TO phonon modes, respectively. The peak at 581 cm^{-1} was attributed to E_1 (LO) mode in nanostructure due to the presence of electric field effects at surfaces,[36] and TO branch of E_1 mode was observed at 419 cm^{-1}. Mode A_1 (LO) usually around 580 cm^{-1} is probably overlapped with E_1 (LO), but for A_1 (TO) mode a weak line observed at 382 cm^{-1} was assigned. Some other weak vibrations observed at 332, 666 and 1154cm^{-1} (not seen in Figure 4) indicate the multi-phonon processes occurring in ZnO.[37] The presence of CoO compounds is indicated by bands centered at around 176, 494, 529, 630, 702 and 721 cm^{-1}. The vibrational mode of CoO can occur in two phases of Co_3O_4 and Co_2O_4 with similar position of Raman modes.[38]

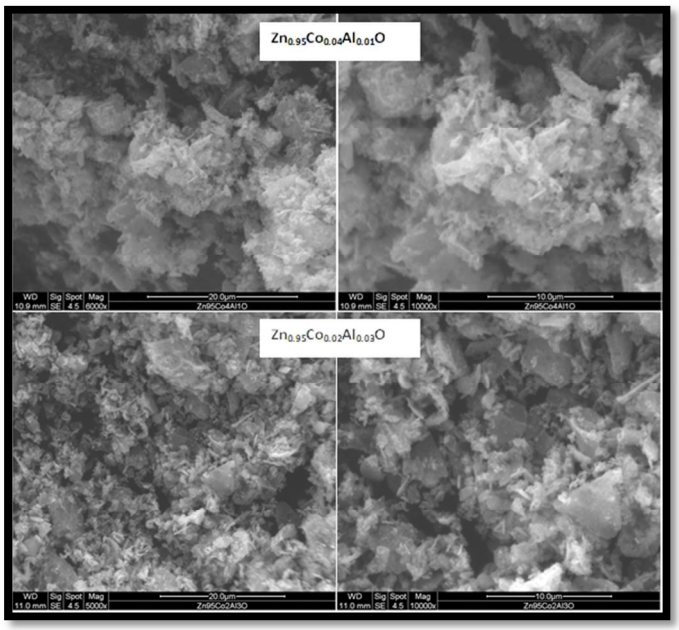

Figure 5. SEM micrographs of the CAZO nanopowder surface.

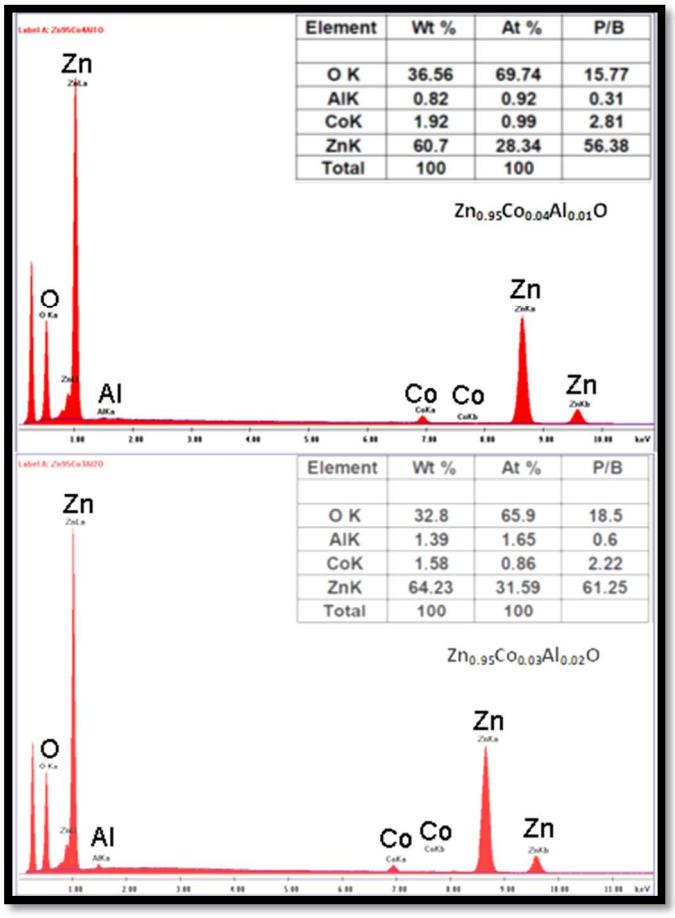

Figure 6. SEM attached EDX spectra of the CAZO nanopowders.

Surface morphology and microstructure: The surface morphologies of the CAZO nanopowders prepared by combustion synthesis are shown in Figure 5. SEM observation reveals that the CAZO nanopowder consists of porous and foam-like morphology. It exhibits a homogenous morphology with porous agglomerated structure. The porosity is assumed to originate in the evaporation of gases during their decomposition. The energy dispersive X-ray spectra (EDX) of the CAZO nanopowders are shown in Figure 6 and report the presence of Zn, Co, Al and O elements. The composition of the nanopowders determined from EDX spectra shows a good agreement with the stoichiometry of the solution.

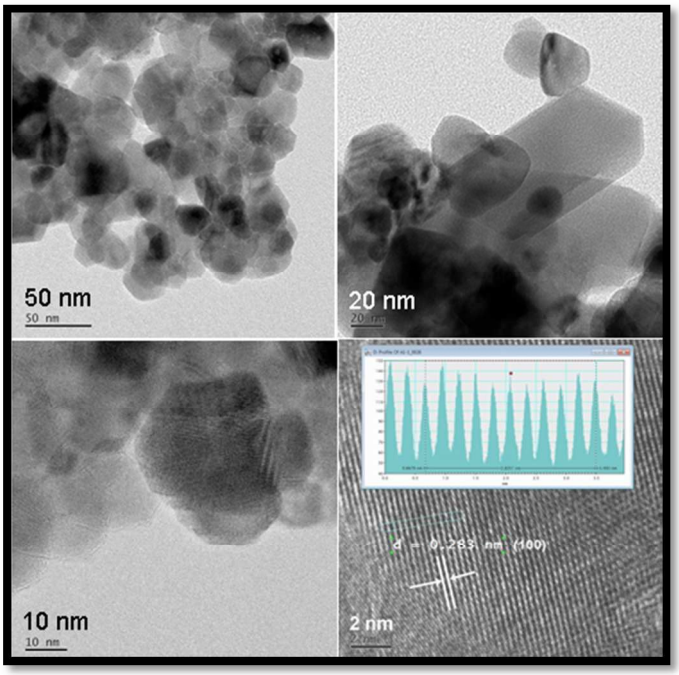

Figure 7. HR-TEM micrographs of the $Zn_{0.95}Co_{0.04}Al_{0.01}O$ nanocrystals.

The morphology, particles size and lattice planes of the CAZO nanocrystals were analyzed by high resolution transmission electron microscopy. The TEM and HR-TEM micrographs are shown in Figure 7 which confirms the formation of hexagonal nanocrystals of ZnO. The size of the hexagonal shaped particles varied in the range of 15 – 30 nm, while few of the nanocrystals grown in z-direction bigger than average (with size ~100nm) were found. The larger crystals are assumed to be early formed nanocrystals which further grew during the combustion and the calcination. Selected Area Electron Diffraction (SAED) patterns were treated by Process Diffraction software.[39] Data treatment included circular integration of SAED intensities from TEM and calibration of the integrated data intensity peaks by means of Camera Length (CL) for comparison and indexation purposes with the standard Powder Diffraction File (PDF). The SAED spectra in Figure 8 confirmed the diffraction of electrons from the ZnO lattice planes. The energy dispersive X-ray spectra (EDX) from TEM were recorded in order to confirm the elements in the composition. The EDX spectra shown in Figure 9 confirmed the presence of Zn, Co, Al and O in the composition.

Apart from these elements, the spectra exhibited some elements such as Cu, C, Si which were present in the carbon coated copper grid used as the sample holder.

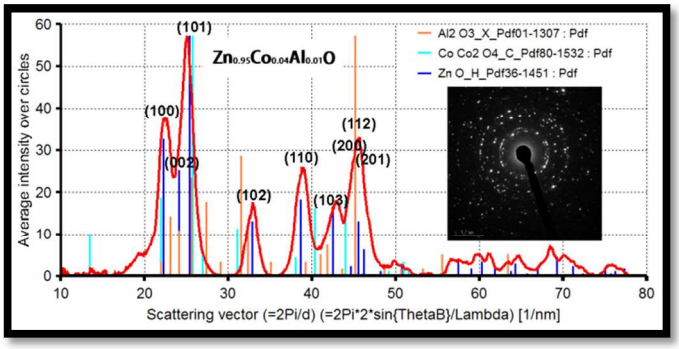

Figure 8. A plot of the comparison between SAED pattern of $Zn_{0.95}Co_{0.04}Al_{0.01}O$ nanocrystals and standard ZnO, Al_2O_3 and Co_3O_4 X-ray diffraction patterns.

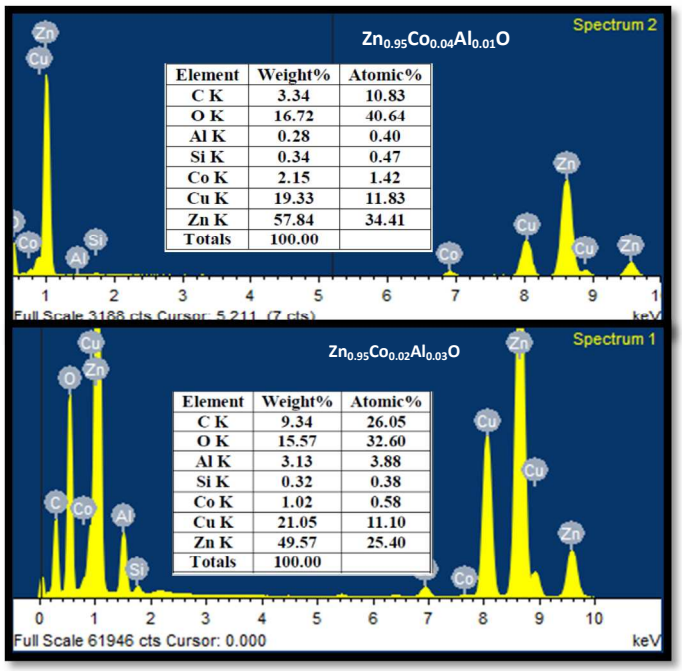

Figure 9. EDX spectra of the CAZO nanocrystals from TEM.

Room temperature ferromagnetism: The room temperature magnetic hysteresis (M-H) curve for the CASO nanoparticles calcined at 600ºC is shown in Figure 10.[14] The M-H curve exhibits ferromagnetic nature with high remnant magnetization with a small coercive field and highly magnetized narrow hysteresis loop.[14] The ferromagnetic hysteresis increases with increase of Co concentration in the CAZO. For the 2 at% of Co, the ferromagnetism was very small; it seems almost like paramagnetic as shown in Figure S7. It was also found that, no saturation magnetization is reached in any of the samples with applied fields, which is ideal for spintronics.

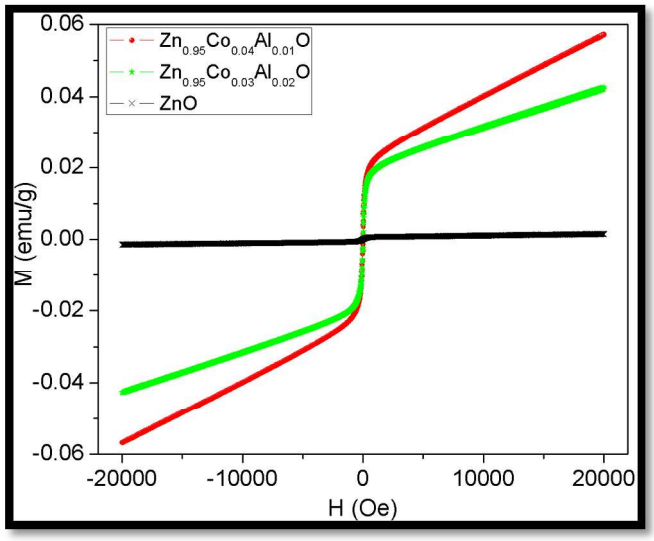

Figure 10. Room temperature ferromagnetic hysteresis curve for the CAZO nanoparticles calcined at 600ºC.[14]

4. CONCLUSIONS

The heterogeneous metal oxide composite nanoparticles of $Zn_{1-x-y}Co_xAl_yO$ were synthesised by CNA combustion method. The prominent strong peaks of ZnO planes were identified from XRD patterns confirm the formation of Co and Al co-doped ZnO nanopowders. Additionally, minute peaks of (222) and (511) planes of Al_2O_3, (220) plane of ZnO_2, and (400) and (440) planes of Co_3O_4 were observed. The presence of the shift in XRD peaks and micro-strains correlate with the doping of Co and Al in Zn sites. We conclude that both, the doping and individual metal-oxides, were formed during the combustion synthesis process. This composition was also confirmed by additional structural analysis performed by means of SAXS/WAXS, Raman and FTIR. The powder morphology, crystallite size, shape and inter-planar distances were analysed by electron microscopy and diffraction. The resulting particle size observed by SAXS was >20nm, which agrees with TEM micrographs. It also matches with the crystallite size observed from XRD profile ranging from 18 to 37 nm. Lattice deformation identified from the shift of XRD peaks corresponds to average micro-strain of about 2.5×10^{-3}. It was concluded that the combustion synthesised powder consists of Co and Al co-doped ZnO ($Zn_{1-x-y}Co_xAl_yO$; i.e., CAZO), and a minute quantities of heterogeneous metal oxide phases of Zn, Co and Al. It was also found that, the CAZO exhibits room ferromagnetic hysteresis, which increases with Co content.

Acknowledgements

The result was developed within the CENTEM project, reg. no. CZ.1.05/2.1.00/03.0088 co-funded by the ERDF as part of Ministry of Education, Youth and Sports OP RDI programme.

Notes and references

[a]*New Technologies Research Centre, University of West Bohemia in Pilsen, Plzeň-30614, Czech Republic, E-mail: rsiddhes@yahoo.com, rajendra@ntc.zcu.cz*

[b]*CEITEC IPM, Institute of Physics of Materials, ASCR, v.v.i., Žižkova 22, CZ-61662 Brno, Czech Republic.*

[*] *Corresponding author: R. Siddheswaran, E-mail: rsiddhes@yahoo.com; rajendra@ntc.zcu.cz; Phone: +420-726914771; Fax: +420377634702.*

Electronic Supplementary Information (ESI) available: [The supporting information shows some figures and information about XRD, SAXS and Raman spectra of CAZO nanopowders, and also contains figures of TEM micrographs of $Zn_{0.95}Co_{0.03}Al_{0.02}O$ and $Zn_{0.95}Co_{0.02}Al_{0.03}O$ nanocrystals.]. See DOI: 10.1039/b000000x/.

References

1 Y. Caglar, A. Arslan, S. Ilican, E. Hur, S. Aksoy, M. Caglar, *J. Alloy. Compd.* 2013, **574,** 104.
2 P.H. Lei, C.M. Hsu, Y.S. Fan, *Org. Electron.* 2013, **14,** 236.
3 Y.J. Li, K.M. Li, C.Y. Wang, C.I. Kuo, L.J. Chen, *Sens. Act. B: Chem.* 2012, **161**, 734.
4 J.B. Lee, H.J. Lee, S.H. Seo, J.S. Park, *Thin Solid Films* 2001, **398**, 641.
5 S. Park, D.W. Lee, J.C. Lee, J.H. Lee, *J. Am. Ceram. Soc.* 2003, **86**, 508.
6 X. Du, Y. Fu, S. Tan, J. Luo, A. Flewitt, S. Maeng, S. Kim, Y. Choi, D. Lee, N. Park, *J. Phys. : Conference Series* 2007, **76**, 012035.
7 R.N. Viswanath, S. Ramasamy, R. Ramamoorthy, P. Jayavel, T. Nagarajan, *Nanostruct. Mater.* 1995, **6**, 993.
8. D. A Dinh, K. N. Hui, K S Hui, J Singh and P. Kumar, *Rev. Adv. Sci. Eng.* 2013, **2,** 259.
9. J. Singh, P. Kumar, K. S. Hui, K. N. Hui, K. Ramam, R.S. Tiwari and O. N. Srivastava, *CrystEngComm,* 2012, **14**, 5898.
10 A. Fouchet, W. Prellier, L. Mechin, *Superlattice Microstr*. 2007, **42**, 185.
11 K. Sato, H.K. Yoshida, *Physica E* 2001, **10**, 251.
12 V.K. Sharma, M. Najim, A.K. Srivastava, G.D. Varma, *J. Magn. Magn. Mater*. 2012, **324**, 683.
13 D.P. Norton, S.J. Pearton, M. Zavada, W.M. Chen, I.A. Buyanova, *Thin Films and Nanostructures: Processing, Properties and Applications,* Elsevier Ltd. Ed. 2006, p555–576.
14 R. Siddheswaran, R.V. Mangalaraja, M.E. Gómez, R.E. Avila, C.E. Jeyanthi, *J. Alloy. Compd.* 2013, **581**, 146.
15 R. Siddheswaran, E.P. Tijerina, M.F. Meléndrez, R.E. Avila, C.E. Jeyanthi, M.E. Gomez, R.V. Mangalaraja, *Spectrochim. Acta A.* 2013, **106**, 118.
16 M.H. Huang, Y. Wu, H. Feick, N. Tran, E. Weber, P.D. Yang, *Adv. Mater.* 2001, **13**, 113.
17 Q. Wan, K. Yu, C.L. Lin, *Appl. Phys. Lett.* 2003, **83**, 2253.
18 Z. Chen, S. Shan, M.S. Cao, L. Lu, S.X. Mao, *Nanotechnology* 2004, **15**, 365.
19 Z. Wang, X.F. Qian, J. Yin, Z.K. Zhu, *Langmuir* 2004, **20,** 3441.
20 Y. Li, G.W. Meng, L.D. Zhang, F. Phillip, *Appl. Phys. Lett.* 2000, **76**, 2011.
21 C.C. Hwang, T.Y. Wu, *Mater. Sci. Eng. B* 2004, **111**, 197.
22. P. Kumar, J. Singh, K. Ramam, R. S. Tiwari, O. N. Srivastava, K Singh and A. C. Pandey, *CrystEngComm,* 2012, **14**, 1653.
23. J. Singh, P. Kumar, K. N. Hui, J. Jung, R. S. Tiwari and O.N. Srivasatva, *RSC Advances,* 2013, **3**, 5465.
24 Y.N. Zhao, M.S. Cao, J.G. Li, Y.J. Chen, *J. Mater. Sci.* 2006, **41**, 2243.
25 S. Ekambaram, S. *J. Alloy Compd.* 2005, **390**, L4.
26 S. Ekambaram, K.C. Patil, *J. Mater. Chem.* 1995, **5**, 905.
27 Y. Tao, G. Zhao, W. Zhang, X. Xia, *Mater. Res. Bull.* 1997, **32**, 501.
28 J.I. Langford, *J. Appl. Cryst.* 1978, **11**, 10.
29 R. Delhez, T.H. Keijser, E.J. Mittemeijer, *Fresenius Z. Anal. Chem.* 1982, **312**, 1.
30 O. Glatter, O. Kratky, *Small Angle X-ray Scattering,* Academic Press Inc., London 1982**.**
31 J. Ilavsky, P.R. Jemian, *J. Appl. Cryst.* 2009, **42**, 347.
32 *COBLENTZ Society*, Data from NIST Standards Reference Database *69*: NIST Chemstry WebBook, by the U.S. Secretary of Commerce on behalf of the United States of America, **2011**. Ref: 4650 *(http://webbook.nist.gov./cgi/cbook.cgi?ID=B6004651&Mask=80).*
33 N.H. Nickel, K. Fleischer, *Phys. Rev. Lett.* 2003, **90**, 197402.
34 U. Rossler, L. Bornstein,. *New Series, Group III. Vol. 17B, 22, 41B.* Ed**. 1999**, Springer, Heidelberg.
35 C.A. Arguello, D.L. Rousseau, S.P.S. Porto, *Phys. Rev.* 1969, **181**, 1351.
36 M. Gabas, P. Dıaz-Carrasco, F. Agullo-Rueda, P. Herrero, *Sol. Energy Mater. Sol. Cells*. 2011, **95**, 2327.
37 Q. Xu, X. Zhu, F. Zhang, L. Yang, W. Jiang, X. Zhou, *Vacuum* 2010, **84**, 1315.
38 B. Hadzic, N. Romcevic, M. Romcevic, I. Kuryliszyn-Kudelska, W. Dobrowolski, J. Trajic, D. Timotijevic, U. Narkiewicz, D. Sibera, *J. Alloy. Compd.* 2012, **540**, 49.
39 J.L. Lábár, *Ultramicroscopy* 2005, **103**, 237.